

**UWL REPOSITORY**  
**repository.uwl.ac.uk**

Displacement monitoring in airport runways by persistent scatterers SAR  
interferometry

Bianchini Ciampoli, Luca, Gagliardi, Valerio, Ferrante, Chiara, Calvi, Alessandro, D'Amico, Fabrizio and Tosti, Fabio ORCID logo ORCID: <https://orcid.org/0000-0003-0291-9937> (2020) Displacement monitoring in airport runways by persistent scatterers SAR interferometry. *Remote Sensing*, 12 (21). p. 3564.

<http://dx.doi.org/10.3390/rs12213564>

This is the Accepted Version of the final output.

**UWL repository link:** <https://repository.uwl.ac.uk/id/eprint/7438/>

**Alternative formats:** If you require this document in an alternative format, please contact: [open.research@uwl.ac.uk](mailto:open.research@uwl.ac.uk)

**Copyright:** Creative Commons: Attribution 4.0

Copyright and moral rights for the publications made accessible in the public portal are retained by the authors and/or other copyright owners and it is a condition of accessing publications that users recognise and abide by the legal requirements associated with these rights.

**Take down policy:** If you believe that this document breaches copyright, please contact us at [open.research@uwl.ac.uk](mailto:open.research@uwl.ac.uk) providing details, and we will remove access to the work immediately and investigate your claim.

**Rights Retention Statement:**

1 Article

## 2 **Displacement monitoring in Airport Runways** 3 **by Persistent Scatterers SAR Interferometry**

4 **Luca Bianchini Ciampoli<sup>\*1</sup>, Valerio Gagliardi<sup>1</sup>, Chiara Ferrante<sup>1</sup>, Alessandro Calvi<sup>1</sup>, Fabrizio**  
5 **D'Amico<sup>1</sup> and Fabio Tosti<sup>2</sup>**

6 <sup>1</sup> Department of Engineering, Roma Tre University, Via Vito Volterra 62, 00146, Rome, Italy

7 <sup>2</sup> School of Computing and Engineering, University of West London, St. Mary's Road, W5 5RF, Ealing,  
8 London, United Kingdom

9 \* Correspondence: luca.bianchiniciampoli@uniroma3.it; Tel.: +39 06 5733 3617

10 Received: date; Accepted: date; Published: date

11 **Abstract:** Deformations monitoring in airport runways and the surrounding areas is crucial,  
12 especially in case of low-bearing capacity subgrades, such as the clayey subgrade soils. An effective  
13 monitoring of the infrastructure asset allows to secure the highest necessary standards in terms of  
14 the operational and safety requirements. Amongst the emerging remote sensing techniques for  
15 transport infrastructures monitoring, the Persistent Scatterers Interferometry (PSI) technique has  
16 proven effective for the evaluation of the ground deformations. However, its use for certain  
17 demanding applications, such a as the assessment of millimetric differential deformations in airport  
18 runways, is still considered as an open issue for future developments. In this study, a time-series  
19 analysis of COSMO-SkyMed satellite images acquired from January 2015 to April 2019 is carried  
20 out by employing the PSI technique. The aim is to retrieve the mean deformation velocity and time  
21 series of the surface deformations occurring in airport runways. The technique is applied to Runway  
22 3 at the “Leonardo da Vinci” International Airport in Rome, Italy. The proposed PSI technique is  
23 then validated by way of comparison with the deformation outcomes obtained on the runway by  
24 traditional topographic levelling over the same time span. The results of this study clearly  
25 demonstrate the efficiency and the accuracy of the applied PSI technique for the assessment of  
26 deformations in airport runways.

27 **Keywords:** Interferometric Synthetic Aperture Radar, InSAR, Permanent Scatterers, PS-InSAR,  
28 Transport Infrastructure Maintenance; Airport runway; Airport monitoring.

---

### 30 **1. Introduction**

31 Runways are central elements in airport infrastructures, as they are mostly dedicated to the two  
32 fundamental and most critical manoeuvres of taking-off and landing of the aircrafts. In light of this,  
33 runways must comply with very strict requirements in terms of the construction [1] and the  
34 maintenance standards [2]. In this regard, it is worthy of mention that a continuously regular surface  
35 must be ensured in runways over their entire life cycle, and no superficial (e.g. cracking or rutting)  
36 or deep (e.g. subgrade subsidence) damage is acceptable to compromise safe manoeuvring of the  
37 aircrafts.

38 Although the provision of proper design methods for runways is crucial to minimise future  
39 maintenance and rehabilitation of the infrastructure, this can be compromised by other critical factors,  
40 such as construction site related issues (e.g. geotechnical instability of the subgrade) or the non-linear  
41 action of different heavy loads over the infrastructure life cycle. The occurrence of these events  
42 requires a dedicated and deep monitoring of differential settlements and deformations of the surface,  
43 in order to plan targeted interventions on time [3, 4] and comply with budget constraints [5].

44 Within this context, it is important to mention that innovative inspection techniques are in  
45 demand by infrastructure agencies and administrators to be incorporated into more effective  
46 infrastructure management systems. Scope is to enhance the reliability of the decay prediction models  
47 by increasing the productivity of the system at reduced inspection costs. Nowadays, various  
48 methodologies have been reported as effective in the detection and monitoring of deformations in  
49 runways. Among these, the most acknowledged techniques are the point-based geodetic methods,  
50 such as the topographic levelling [6], often coupled to Global Navigation Satellite Systems (GNSS)  
51 for referencing purposes [7], or the LiDAR technique [8]. These methods work with different  
52 resolutions and they all rely on the comparison between the positions of points measured across  
53 successive surveys. This approach is necessary to allow the monitoring of the deformation trend of  
54 the targets.

55 More recently, satellite-based techniques are gaining momentum for the monitoring of transport  
56 infrastructures. One of their major advantage is on the fact that measurements of targets can be  
57 repeated over an investigated area, with a fixed revisiting time that is related to the orbit of the  
58 satellite. This allows to collect a significant amount of information regularly distributed in time,  
59 without the requirement to close the infrastructure to traffic. Hence, tremendous benefits can be  
60 brought forward in terms of safety- and costs in the asset management process [9]. Among the  
61 satellite remote sensing techniques, the Synthetic Aperture Radar Interferometry (InSAR) has proven  
62 effective in the analysis of subsidence effects in a wide range of structures [10] and infrastructures  
63 [11].

64 This study focuses on the application of the InSAR technology and, more specifically, of the  
65 Persistent Scatters Interferometry (PSI) [12, 13] to the monitoring of differential settlements in airport  
66 runways. To demonstrate the viability of the proposed technique, a case study is presented with an  
67 application to Runway 3 at the “Leonardo da Vinci” International Airport in Rome, Italy. The  
68 investigated area is known to be affected by subsidence due to soft subgrades. Results of the InSAR  
69 acquisitions and processing are finally compared to the deformations obtained on the runway by  
70 traditional topographic levelling over the same time span.  
71

## 72 **2. Aim and Objectives**

73 The main aim of the investigation reported in this paper is to verify the effectiveness of the  
74 satellite remote sensing technology in gaining vital information about the functionality of airport  
75 runways for inclusion in airport asset management systems. To achieve this aim, the following  
76 objectives are identified:

- 77 • to assess runway displacements at the millimetre scale and evaluate their trend on a  
78 multi-year scale using the PSI monitoring technique;
- 79 • to compare the results obtained with the PSI technique and the traditional topographic  
80 levelling method.

## 81 **3. Runway monitoring techniques**

82 Relevant methods employed for the monitoring of airport runways are presented in the  
83 following sections. The topographic levelling and the LiDAR techniques are here referred to as  
84 “established techniques”, as opposed to the PSI method, referred to as an “innovative technique”.

### 85 **3.1 Established Techniques**

#### 86 *Topographic levelling*

87 The process of measuring variations in elevation is a relatively basic operation in topographical  
88 surveys, and it is typically referred to as levelling. Various levelling techniques have been developed  
89 over the time. In regard to infrastructure surveying, geometric levelling is the most adopted [14]. The  
90 height difference is here obtained from readings on levelling staffs where the level’s horizontal  
91 sightline intersects them. The level is mostly used in the middle between two levelling staffs

92 (differential levelling), with the objective of the survey being the definition of the difference in vertical  
93 distance between the two staff positions.

94 As demonstrated by [6], the topographic levelling procedure allows to monitor the long-term  
95 settlements of an infrastructure by measuring the variation in the vertical position of the target over  
96 multiple surveys. This is performed with respect to a single or multiple stable point, typically referred  
97 to as topographic benchmarks.

98 In the last decades, various levelling investigations on civil infrastructures have been reported  
99 in the literature [15, 16]. In regard to the monitoring of the airport runways, both advantages and  
100 drawbacks can be mentioned on the use of the topographic levelling. As for the advantages, the high  
101 accuracy of the measurements [17] and the possibility to perform tests independently from indoor or  
102 outdoor environments once a reference point is defined [18] is worthy of mention. The drawbacks  
103 include a) a limited productivity [19, 20], due to the need of measuring each target separately, b) the  
104 necessity to close the runway during testing, c) the impossibility to perform the survey in adverse  
105 weather conditions [15] and d) the provision of a clear line of sight between consecutive targets of  
106 the survey, implying several practical constraints. Lastly, the observed displacements are relative  
107 measurements that might be affected by potential settlements levelling benchmarks, which may  
108 result in a distortion of the results.

### 109 *LiDAR Surveys*

110 LiDAR is a surveying method that measures the distance to a target by illuminating the target  
111 with a laser light and measuring the reflected light with a sensor [21]. The differences in the laser  
112 return, times and wavelengths can then be used to create digital 3-D representations of the target.  
113 Since this technology has started to spread in several scientific and professional fields, successful  
114 applications in transport infrastructures monitoring have been reported [22] for both the static [23]  
115 and the mobile [24] configurations of the equipment.

116 With regard to airport runway monitoring, static terrestrial laser scanners are being mostly used  
117 for reconstructing the geometry of the pavement surface in order to detect defects and decayed areas  
118 [8, 25]. This is carried out by illuminating the whole runway surface by means of different scans  
119 performed at different and distributed survey stations. A certain rate of superposition of the point  
120 clouds must be also provided for matching purposes [26]. The georeferencing operation between  
121 different scans is ensured by the use of common ground targets working as reference objects.  
122 However, by coupling a GNSS receiver to this ground targets, it is possible to skip from relative to  
123 global coordinates and compare successive surveys, in order to monitor the evolution of differential  
124 settlements.

125 Among the advantages of this technique, it is worth to mention the rapidity and the high  
126 resolution of the surveys, as millions of point clouds can be collected in limited time. Furthermore,  
127 the use of global georeferenced ground targets allows to prevent the measurements from relative  
128 errors due to the instability of the reference. In turn, LiDAR surveys require the runway to be closed  
129 to traffic during the tests. In addition, the application of this technique, as well as the levelling,  
130 requires the presence of operators on site. This represents a considerable safety concern as airport  
131 runways and aprons are considered as high-risk environments.

### 132 *3.2 Persistent Scatterers Interferometry (PSI)*

133 The InSAR technique, or SAR interferometry, relies on the measurement of the signal phase  
134 variation between images acquired by a satellite orbiting over the same area [9]. Indeed, once the  
135 phase contribution related to atmospheric conditions and both temporal and spatial decorrelations  
136 are adequately accounted for, it is possible to detect a time sequence of the sensor–target distance  
137 along the sight direction of the satellite. This can be related to the surface deformations, e.g., the  
138 subsidence. [11].

139 For this purpose, various processing techniques have been proposed over time. Among these,  
140 PSI is one of the most acknowledged [12, 13]. PSI is based on the statistical analysis of the signals  
141 back-scattered from a network of phase-coherent targets, namely the Persistent Scatterers (PSs) and

142 defined as the points on the ground returning stable signals to the satellite sensor. Indeed, the  
143 constant scattering properties of the PS over time and the reflection dominance within a pixel cell are  
144 effective in reducing the temporal and geometric decorrelations. In addition, the atmospheric  
145 contribute can be estimated and removed using the series of images acquired at different times.

146 SAR sensors operate at different bands of the microwave domain, namely X, C and L,  
147 corresponding to wavelengths ( $\lambda$ ) ranging from 2.4 to 30 cm. Each wavelength is associated to a  
148 differently sized resolution cell on the ground, whose displacement trend is described by a single PS.

149 By means of the PSI technique, satellite remote sensing can provide a continuous monitoring of  
150 the overall stability of structures and infrastructures, as well as the surrounding environment. This  
151 is obtained by the analysis of multiple SAR images collected at different time stages. Subject-related  
152 literature reports the SAR techniques as viable tools for the monitoring of ground deformations,  
153 landslides, subsidence and tectonic motions [27-29]. Similarly, in the last few years, various successful  
154 applications of the PSI technique have been presented, proving the feasibility of this technique for  
155 the assessment of transport infrastructures and surveillance areas, such as highways [30-32], bridges  
156 [33-37], subways and tunnels [31, 38-39], railways [40-43], and airport runways [44-46]. This evidence  
157 confirms the wide applicability of these techniques within these specific areas of endeavour.

158 The use of the InSAR technique in transport infrastructures monitoring holds several advantages  
159 [9]. InSAR data can be collected regardless of the atmospheric and lighting conditions. In addition, a  
160 single InSAR survey permits the analysis of extended areas, due to the wide footprint of the sensor.  
161 The continuous motion of the satellites ensures the availability of regularly spaced images, which  
162 allows to perform very dense analyses as opposed to on-site and low-frequency inspections. The  
163 acquisition and processing of SAR images do not require on-site operations, thereby preventing both  
164 the closure of the runway to air traffic and the presence of operators on the site, with related economic  
165 and safety benefits.

166 On the opposite, the applicability of the PSI analysis is by definition limited to areas where an  
167 adequate number of PSs can be observed. This implies that, in case of varying surface conditions (e.g.  
168 frequent repaving or accelerated degradation), the stability of the scattering properties of the target  
169 may be compromised, with a reduced number of PSs being detected. Furthermore, reliable InSAR  
170 assessments require the processing of various SAR images in order to detect statistically stable PSs.  
171 This occurrence involves potential computational-related issues, due to the size of database required  
172 at each survey. Lastly, according to the frequency of the adopted sensor, uncertainties may arise in  
173 the scattering source, as it is impossible to recognise the scattering object within the resolution cell.

## 174 4. Case Study

### 175 4.1 Site Description

176 In the present study, a case study is presented where the PSI technique is applied Runway 3 at  
177 the "Leonardo da Vinci" International Airport in Rome, Italy.

178 The airport is located in the area of Fiumicino, about 30 kilometres on the west of Rome, and  
179 carries most of the intercontinental air traffic from and towards Italy, that rank it as one of the major  
180 airports in Europe. With in excess of 43 million passengers in 2018 and over 199000 tons of traffic, the  
181 airport is the largest in Italy by number of passengers/year and ranks second by number of cargo  
182 flights/year.

183 The airport has three terminals reserved for domestic, international and intercontinental flights  
184 and three runways. Initially, the layout of the airport included two runways (Runway 1 and Runway  
185 2) only. However, due to an increasing traffic demand, it was expanded with a new runway located  
186 in the north-east area of the airport, that develops in the north-south direction (Fig. 1)

187



188

189 **Figure 1.** Satellite view of “Leonardo Da Vinci” International Airport and location area of Runway 3 (Google  
190 Earth Image – 2015)

191 The area where Runway 3 was realized is known to be affected by the presence of clayey and  
192 peaty soils. As a result, the runway is interested by long-term differential subsidence effects, which  
193 required accurate monitoring and brought to a full-depth pavement rehabilitation in 2015. This was  
194 aimed to increase the bearing capacity of the subgrade in the norther section of the runway, where  
195 severe differential settlements had been recorded in the previous years. Nevertheless, Runway 3  
196 remains a critical asset that is levelled every year in order to be able to monitor the deformation trends  
197 and plan maintenance activities.

#### 198 *4.2 Levelling Data*

199 In regard to the on-site topographic surveys conducted on the survey area, a classical geometric  
200 levelling survey of the runway was conducted by means of the DNA03 Digital Level system,  
201 manufactured by Leica. The elevation measurements were collected by means of a 2 m high levelling  
202 rod made of invar, i.e. a metal with a limited thermal expansion coefficient. The main features of the  
203 employed levelling system are summarised in Tab.1.

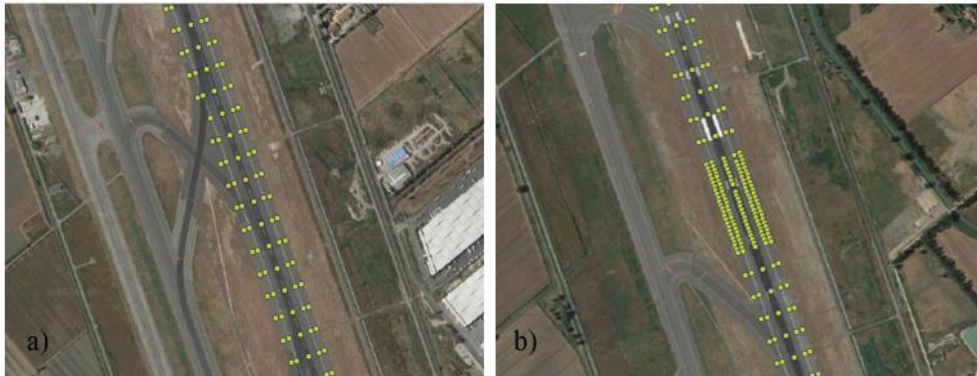
204 **Table 1.** Main features of the employed levelling equipment

	Leica DNA03
<b>Measuring Range</b>	Up to 110 m
<b>Measuring Time</b>	Operator Dependent
<b>Levelling Accuracy (Std Dev.)</b>	±0.3 mm/km
<b>Compensator</b>	Pendulum with magnetic damping
<b>Display</b>	LCD

205 In particular, in-situ levelling data were collected by multiple closed-loop levelling nets covering  
206 the entire Runway 3. The collected nets were automatically compensated, with an average Squared  
207 Root Mean Error of 0.94 mm. The starting and ending point of the measure was a levelling benchmark  
208 located in the north-west corner of the runway area, which was verified to be stable in elevation. This  
209 point was connected to the high precision levelling net developed by the Istituto Geografico Militare  
210 (IGM), through a levelling line having an average accuracy of 1.0 mm/km.

211 Tests were performed every year from 2015 to 2019 and covered five sections along the runway  
212 with a transversal spacing of 15 metres and a length equal to the entire runway longitudinal  
213 development (Fig. 2).

214 Furthermore, the output of these data allows to detect and exactly quantify the displacements  
 215 and the average-velocity in the investigated time period. Therefore, this information turns out to be  
 216 significant for a validation of the displacements detected by the InSAR technique.



217  
 218 **Figure 2.** Scheme of in-situ levelling data: a) section in the middle region of Runway 3; b) increase of  
 219 measuring points density on the ground in the area interested by subsidence effects

### 220 4.3 SAR Imagery

221 In regard to the application of the InSAR technique, a multi-temporal interferogram analysis of  
 222 SAR images, namely the Persistent Scatterers Interferometry technique (PSI), was applied. To this  
 223 effect, two different data-stacks were acquired in Ascending and Descending geometries using high-  
 224 resolution SAR imagery acquired in X-Band, that allows detection of displacements with a millimetre  
 225 accuracy.

226 In more detail, a dataset of 72 Stripmap images collected in Ascending and Descending  
 227 geometries from the COSMO-SkyMed mission (COSMO-SkyMed Product - ©ASI: Italian Space  
 228 Agency, 2015-2019, All Rights Reserved) were processed. The system operates in X-band  
 229 corresponding to a wavelength of 3.1 cm, with a 3 m ground-resolution cell. The radar antenna is a  
 230 phased array that is 1.4 m wide x 5.7 m long. The system is capable of both single- and dual-  
 231 polarisation data collection. The central frequency is 9.6 GHz with a maximum radar bandwidth of  
 232 400 MHz. The main features of the SAR dataset are reported in Tab. 2.

233 **Table 2.** Main features of the SAR imagery dataset from the COSMO-SkyMed mission - Italian Space  
 234 Agency (ASI)

	Ascending Geometry	Descending Geometry
<b>Number of Images</b>	35	37
<b>Reference Period</b>	01/ 2015–04/2019	03/ 2016–04/2019
<b>Frequency / Wavelength</b>	9.6 GHz / 3.1 cm	
<b>Ground-Range Resolution</b>	3 m	
<b>Azimuth Resolution</b>	3 m	

### 235 4.4 Data Processing

236 These products have been acquired and processed using the PS technique of SARscape  
 237 Interferometric Stacking Module, integrated in the Envi software, within the framework of the project  
 238 “MOBI: MOnitoring Bridges and Infrastructures networks” (proposal ID 46829), approved by the  
 239 European Space Agency (ESA).

240 The processing algorithm includes the following steps [12-13, 48-49]:

- 241 • Generation of differential interferograms out of the stack of SAR images;
- 242 • Implementation of High definition Digital Elevation Models (DEM) for topographic
- 243 phase-term removal;

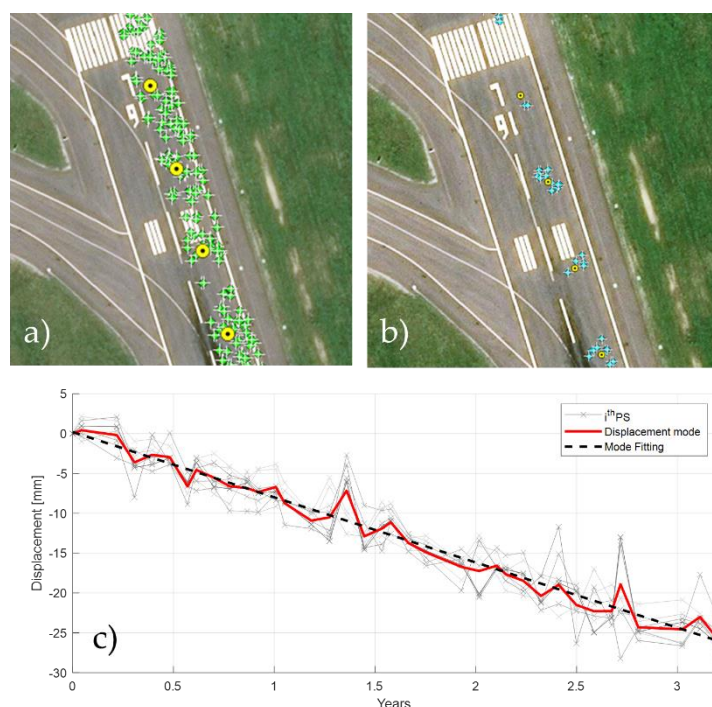
- 244
- 245
- 246
- 247
- 248
- 249
- 250
- Selection of candidate PS points, through the calculation of the Amplitude Dispersion Index;
  - Coherence-based filtering of the dataset;
  - Phase unwrapping;
  - Identification and removal of the phase values not related to the displacements: evaluation of spatial, orbital and atmospheric decorrelations;
  - Identification of the displacements and calculation of deformation time series.

251 In regard to the implementation of the high definition DEM models, an SRTM v3 “Shuttle Radar  
252 Topography Mission” DEM was collected and implemented in the interferometric process [50-51] in  
253 order to identify and subtract phase-related parameters linked to the topography of the investigated  
254 area. The DEM, with a pixel resolution of 3 arc-second (90 m × 90 m), is made available by NASA in  
255 partnership with the United States Geological Survey (USGS) [50].

256 The outputs of the PSI processing algorithm were exported into a GIS environment and the PSs  
257 were displayed as a function of the average annual-motion velocities.

258 A specific procedure was adopted in order to compare each ground-truth levelled data with a  
259 single satellite-derived displacement measure, as follows:

- 260
- 261
- 262
- 263
- 264
- 265
- all the PSs in the vicinity of the observed levelled point are selected within a distance radius of 10 m (Fig. 3a,b);
  - out of all the selected PSs, a single displacement time-series is derived by calculating the moving average of the deformations at each acquisition date (Fig. 3c);
  - the displacement velocity is defined by a linear regression of the displacement against time (Fig. 3c).



266

267 **Figure 3.** Scheme of SAR data processing: a) visualisation of the whole PS (green) and Levelling (yellow)  
268 datasets; b) selection of PSs (blue) within a 10 m radius from each levelling point (yellow); c) reconstruction of a  
269 single time-series and deformation velocity starting from the PS sample.

270 Finally, in order to obtain continuous average-velocity maps representative of the runway  
271 condition, a geo-statistical gridding method was implemented both to the PS datasets and the  
272 levelling measurements.

273 The geo-statistical ordinary Kriging method was used for this purpose [52-53]. Kriging is applied  
274 due to the flexibility and the high accuracy in the gridding methods and the provision of

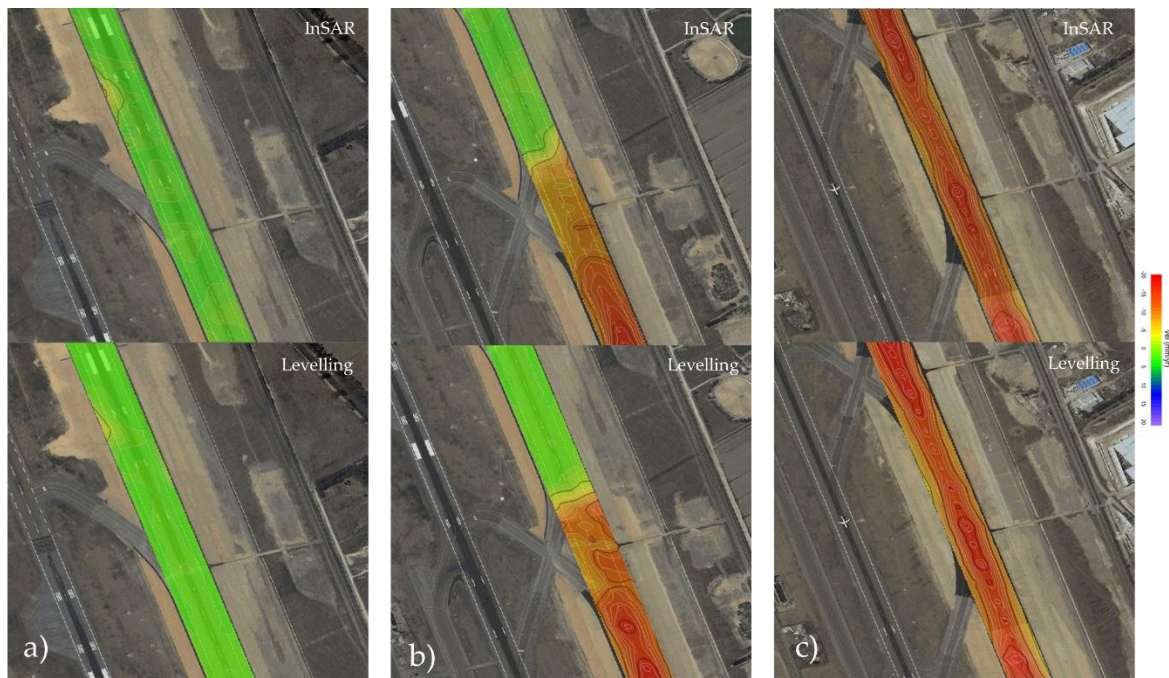
275 representative maps applied to different types of datasets. Moreover, it can compensate for clustered  
 276 data by weighting less the cluster in the overall prediction. Each grid node value is based on the  
 277 known data-points neighbouring the node. Each data point is weighted by its distance away from  
 278 the node and, consequently, points that are further from the node will be weighted less in the  
 279 estimation of the node. To compute the  $Z(x_0)$  value at a randomly-given grid node at position  $x_0$ , the  
 280 following equation is used [52-53]:

$$281 \quad \hat{Z}(x_0) = [w_1 \ w_2 \ \dots \ w_n] \cdot \begin{bmatrix} Z_1 \\ \dots \\ Z_n \end{bmatrix} = \sum_{i=1}^n w_i(x_0) \times Z(x_i)$$

282 where  $\hat{Z}(x_0)$  is the estimated value of the grid node,  $n$  is the number of neighbouring data values  
 283 used in the estimation,  $Z(x_i)$  is the observed value at the  $i^{\text{th}}$  location weighting  $w_i(x_0)$  with  $i$  ranging  
 284 between 1 and  $n$ . The values of the weights add up to 1 in order to ensure that no bias occurs towards  
 285 clustered data points. The weights are intended to summarise two important procedures in a spatial  
 286 inference process, i.e., i) to reflect the structural-proximity of the samples to the estimation location;  
 287 ii) on parallel, they should not have a separation effect, in order to avoid bias effects caused by  
 288 potential sample clusters.

## 289 5. Results

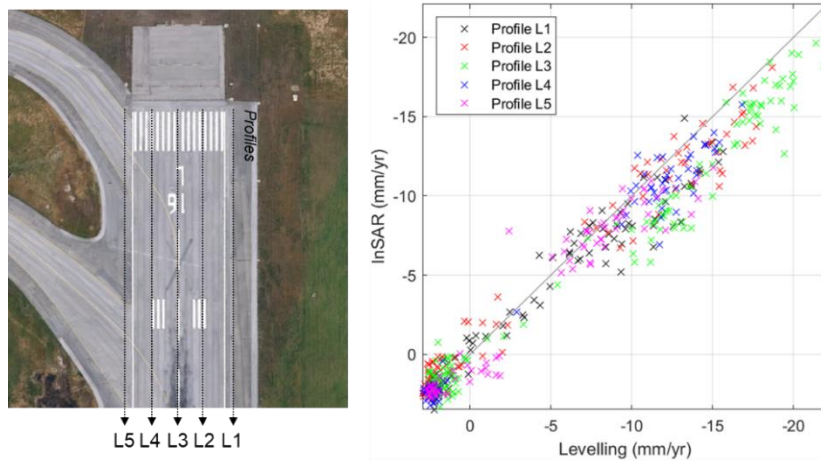
290 As a qualitative assessment of the reliability of the PSI technique, Fig. 4 shows the velocity maps  
 291 obtained from the levelling and the PSI techniques by interpolation of the displacement velocity data.  
 292 The similarity between the two maps in low (Fig. 4a), intermediate (Fig. 4b) and severe (Fig. 4c)  
 293 displacing conditions demonstrates the accuracy of the prediction made using the satellite  
 294 measurements.



295

296 **Figure 4.** Comparison between the velocity maps obtained by (top) PSI datasets and (bottom) levelling,  
 297 relative to a) low (from 2600 m to 3200 m in N direction), b) intermediate (from 1900 m to 2600 m in N  
 298 direction) and c) severe (from 850 m to 1620 m in N direction) displacing conditions

299 A quantitative analysis of the results (see Fig. 5), shows a displacement velocity scatter plot of  
 300 the whole ensemble of survey points, where points belonging to different longitudinal survey profiles  
 301 are marked with different colours. A relatively good matching is observed between levelling and PSI  
 302 across all the five survey sections acquired by levelling, which returned paired values distributed  
 303 very close to the bisector, regardless of the value of velocity.



304

305

**Figure 5.** Displacement velocity scatter plot comparing observed (levelling) and predicted (PSI) data

306

The correlation and the loss performance of the prediction are reported in Tab. 3. This includes Pearson’s coefficients ( $r$ ) and Root Squared Mean Error (RSME) values for the five survey profiles.

307

308

**Table 3** Summary of the PSI potential in predicting levelling results

Survey Profile	$r$ (-)	RSME (mm/yr)
L1	0.9731	1.6430
L2	0.9837	1.6931
L3	0.9857	2.3477
L4	0.9907	1.3247
L5	0.9681	1.5361

309

It is worthy to note that the survey profile L3 returns slightly less accurate results, as shown in both Fig. 5 and Tab. 3. Especially for the highest values of velocity (which are mainly included within L3), the PSI method seems in fact to underestimate the ground-truth levelled displacement trend. The nature of this coherent error is most likely related to the atmospheric noise contribution, which seems not to be completely filtered out through the applied processing [53, 54]. However, the extent of the error is found to be quite limited (around 0.5 cm/year, approximatively). Accordingly, it is observed that the potential of the method in reconstructing the deformation behaviour of the runway is not significantly affected. This allows the provision of very useful information to airport managers for scheduling flight-lists and plan strategic on-site monitoring operations.

310

311

312

313

314

315

316

317

318

As a further confirmation of the above observations, Figure 6 shows the displacement velocity of the survey profiles against the space (WGS84 N Coordinate). Still, it is possible to note that as the displacement trend reaches values higher than 15 mm/year (Fig. 6 b,c,e), the PSI method turns out to slightly underestimate the deformation rate. However, besides this specific observation, Fig. 6 succeeds in demonstrating the effectiveness of PSI in reconstructing the actual deformation pattern over the inspected infrastructure.

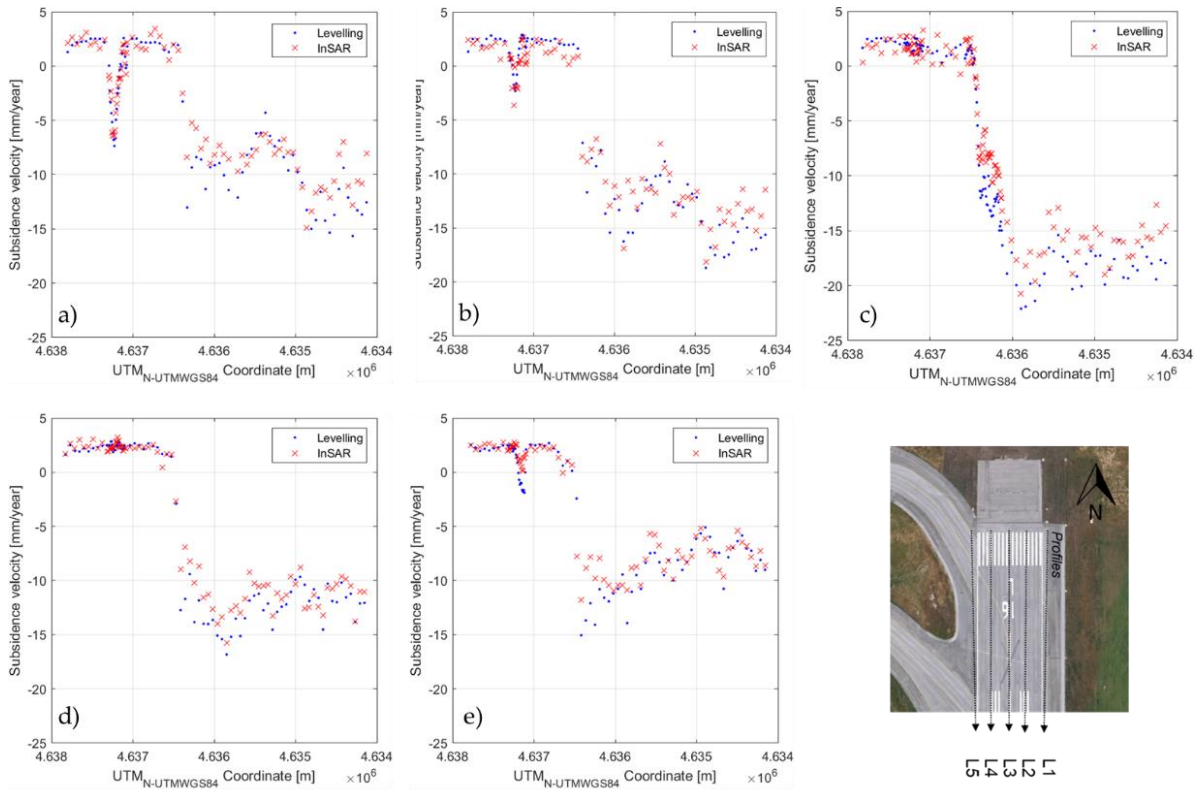
319

320

321

322

323



324

325

**Figure 6.** Displacement velocity trends for longitudinal survey profiles a) L1 to e) L5

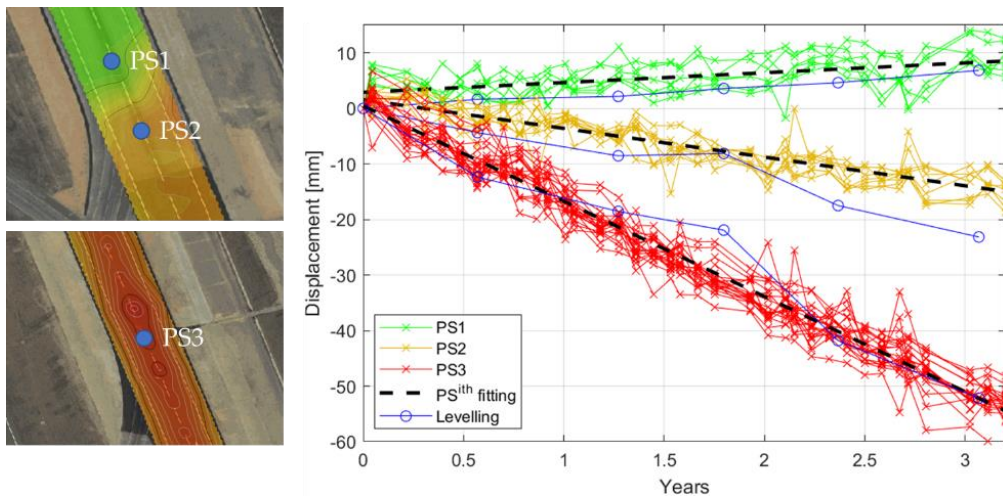
326

327

328

329

In order to evaluate the capability of the method to reconstruct the exact deformation time-series of each levelled point, a few examples are here reported, with reference to the three displacement conditions mentioned in Fig. 4. More specifically, PS1, PS2 and PS3 in Fig. 7 refer to low, intermediate and severe displacement conditions, respectively.



330

331

332

**Figure 7.** Deformation time-series for three points related to low, intermediate and severe displacement conditions

333

334

335

336

337

A quantitative analysis of the comparison between the two methods is instead reported in Tab. 3. Specifically, for every levelled point, the displacement rate is reported for both the survey methodology, with the reliability of the InSAR measurement being expressed by the Root Squared Mean Error.

338 **Table 4** Quantitative analysis of the comparison between InSAR and levelling for the three PS in the  
 339 example

Surveyed Point	Displacement velocity by levelling (mm/yr)	Displacement velocity by InSAR (mm/yr)	RSME (mm)
PS1	1.68	1.76	2.4659
PS2	-6.21	-5.16	4.9875
PS3	-16.93	-17.16	3.9101

#### 340 4. Conclusions

341 This work demonstrates the applicability of the high-resolution X-band COSMO-SkyMed  
 342 mission data and the Persistent Scatters Interferometry (PSI) technique in monitoring the  
 343 deformations occurring on airport runways.

344 To this purpose, a time-series analysis of a set of satellite images acquired from January 2015 to  
 345 April 2019 is carried out by employing the PSI technique. To assess the actual reliability of the method  
 346 in reconstructing the exact deformation pattern of the monitored infrastructure, the outcomes from  
 347 the PSI technique were compared to those obtained by the traditional topographic levelling  
 348 technique, which has been applied on the runway at the same time range as the satellite analysis.

349 The outcome of the analysis clearly indicates that the use of the PSI technique is reliable and  
 350 accurate for deformation assessment purposes.

351 More specifically, the application of the PSI technique has proven effective in reconstructing the  
 352 average trend of the annual deformation velocity (see the coloured maps in Fig. 4 and the profiles  
 353 reported in Fig. 6) and the monthly deformation time-series of each levelled point (see the examples  
 354 included in Fig. 7).

355 As opposed to the advantages related to the application of this method, it is fair to comment that  
 356 in the case of the highest rates of deformation observed in the investigated runway, the PSI technique  
 357 was found to slightly underestimate the subsidence velocity. Such a coherent bias was related to a  
 358 limited processing of the atmospheric noise contribution and, as a consequence, it is expected to be  
 359 accounted for by means of an advanced processing phase.

360 In general, the results presented in this research demonstrate that the PSI technique is worthy of  
 361 implementation in Airport Pavement Management Systems (APMS), which may profit by a  
 362 significant increase of the efficiency in the scheduling of maintenance operations.

363

364 **Author Contributions:** conceptualization, L.B.C. and A.C.; methodology, A.C. and F.D.; investigation, V.G. and  
 365 C.F.; data curation, L.B.C. and F.D.; writing—original draft preparation, L.B.C. and F.T.; writing—review and  
 366 editing, F.D., A.C. and F.T.

367 **Acknowledgments:** The license for using the software ENVI SARscape® is granted by the ESA (European Space  
 368 Agency) approved project "MOBI: MONitoring Bridges and Infrastructure networks" (EOhops proposal ID  
 369 52479). The COSMO-SkyMed Products® - ©ASI: Italian Space Agency, 2015-2019, All Rights Reserved- are © of  
 370 the ASI (Italian Space Agency) delivered under the license to use. The research is supported by the Italian  
 371 Ministry of Education, University and Research under the National Project "Extended resilience analysis of  
 372 transport networks (EXTRA TN): Towards a simultaneously space, aerial and ground sensed infrastructure for  
 373 risks prevention", PRIN 2017, Prot. 20179BP4SM. In addition, the authors express their deep gratitude to G.R.S.  
 374 S.r.l. for providing the topographic levelling database, and for the valuable contribution in interpreting the  
 375 results.

376 **Conflicts of Interest:** The authors declare no conflict of interest.

#### 377 References

- 378 1. Federal Aviation Administration (FAA), Advisory Circular AC 150/5370-10H - Standard Specifications for  
 379 Construction of Airports, 2018

- 380 2. Federal Aviation Administration (FAA), Advisory Circular AC 150/5320-6F - Airport Pavement Design and  
381 Evaluation, **2016**
- 382 3. Li, D., Selig, E.T., Cumulative plastic deformation for fine-grained subgrade soils, *Journal of Geotechnical*  
383 *Engineering*, **1996**, 122 (12), 1006-1013.
- 384 4. Zhou, J., Gong, X., Li, J., Experimental study on saturated soft clay under cyclic loading, *Industrial*  
385 *Construction*, 2000, 30 (11).
- 386 5. Bevilacqua, M., Braglia, M., The analytic hierarchy process applied to maintenance strategy selection,  
387 *Reliability Engineering and System Safety*, **2000**, 70, 71-83
- 388 6. Cosser, E., Roberts, G.W., Meng, X., Dodson, A.H., Measuring the Dynamic Deformation of Bridges Using  
389 a Total Station, Proceedings, 11th FIG Symposium on Deformation Measurements, Santorini, Greece, **2003**
- 390 7. Chen, W., Yuan, J., Li, M., *Application of GIS/GPS in Shanghai Airport Pavement Management System*,  
391 *International Workshop on Information and Electronics Engineering (IWIEE)*, Elsevier, 2012
- 392 8. Barbarella, M., De Blasiis, M.R., Fiani, M., Terrestrial laser scanner for the analysis of airport pavement  
393 geometry, *International Journal of Pavement Engineering*, **2019**, 20(4), 466-480.
- 394 9. Bianchini Ciampoli, L. Gagliardi, V., Clementini, C., Latini, D., Del Frate, F., Benedetto, A., Transport  
395 Infrastructure Monitoring by InSAR and GPR Data Fusion, *Surveys in Geophysics*, **2020**, 41, 371-394.
- 396 10. Bru, G., Herrera, G., Tomás, R., Duro, J., de la Vega, R., Mulas, J., Control of deformation of buildings  
397 affected by subsidence using persistent scatterer interferometry, *Structure and Infrastructure Engineering*,  
398 **2013**, 9 (2), 188-200.
- 399 11. Koudogbo F, Urdiroz A, Robles JG, Chapron G, Lebon G, Fluteaux V, Priol G., Radar interferometry as an  
400 innovative solution for monitoring the construction of the Grand Paris Express metro network—first  
401 results. In: World tunnel conference, 2-25 April, Dubai, **2018**
- 402 12. Ferretti, A., Prati, C., Rocca, F., Nonlinear subsidence rate estimation using permanent scatterers in  
403 indifferential SAR interferometry. *IEEE Transactions on Geoscience and Remote Sensing*, **2000**, 38(5), 2202-  
404 2212.
- 405 13. Ferretti, A., Prati, C., Rocca, F., Analysis of permanent scatterers in {SAR} interferometry, *IEEE Transactions*  
406 *on Geoscience and Remote Sensing*, 2000, 39(1):761 – 763.
- 407 14. Elhassan, I., Ali, A.S., Comparative study of accuracy in distance measurement using: Optical and digital  
408 levels, *Journal of King Saud University – Engineering Sciences*, 23, 15-19, 2011
- 409 15. Kuhlmann, H. and Glaser, A., Investigation of New Measurement Techniques for Bridge Monitoring, 2nd  
410 Symposium on Geodesy for Geotechnical and Structural Engineering, Berlin, Germany, **2002**.
- 411 16. Uddin, W., Gutelius, B., Parrish, C., Airborne Laser Survey Specifications and Quality Management  
412 Protocols for Airport Obstruction Surveys, *Transportation Research Record: Journal of the Transportation*  
413 *Research Board*, **2011**, No. 2214, pp. 117-125.
- 414 17. Hill, C. D. and Sippel, K. D., Modern Deformation Monitoring: A Multi Sensor Approach, FIG XXII  
415 International Congress, Washington DC, USA, **2002**.
- 416 18. Radovanovic, R. S. and Teskey, W. F., Dynamic Monitoring of Deforming Structures: GPS verses Robotic  
417 Tacheometry Systems, The 10th FIG International Symposium on Deformation Measurements, Orange,  
418 California, USA, **2001**
- 419 19. Meng, X., Real-time Deformation Monitoring of Bridges Using GPS/Accelerometers," PhD thesis,  
420 University of Nottingham, Nottingham, UK, **2002**
- 421 20. Uddin, W., Al-Turk, E., Airport obstruction space management using airborne LIDAR three dimensional  
422 digital terrain mapping, Federal Aviation Administration Technology Transfer Conference, **2002**
- 423 21. Kim, J.S., Lee, J.C., Kang, I.J., Cha, S.Y., Choi, H., Lee, T.G., Extraction of geometric information on highway  
424 using terrestrial laser scanning technology. *International Archives of the Photogrammetry, Remote Sensing*  
425 *and Spatial Information Sciences*, **2008**, 37 (B5), 539-544.
- 426 22. Williams, K., Olsen, M.J., Roe, G.V., Glennie, C., Synthesis of transportation applications of mobile LIDAR.  
427 *Remote Sensing*, **2013**, 5 (9), 4652-4692.
- 428 23. Laurent, J., Hebert, J.F., Lefebvre, D., Savard, Y., Using 3D laser road profiling sensors for the automated  
429 measurement of road surface conditions. In: A. Scarpas, N. Kringos, I.A. Al-Qadi, eds. 7th RILEM  
430 international conference on cracking in pavements, mechanisms, modeling, testing, detection and  
431 prevention case histories, Vol. 4, 2012. Dordrecht: Springer, 157-167, **2012**.

- 432 24. Pu, S., et al., Recognizing basic structures from mobile laser scanning data for road inventory studies. *ISPRS*  
433 *Journal of Photogrammetry and Remote Sensing, Supplement Advances in LIDAR Data Processing and*  
434 *Applications*, **2011**, 66, S28–S39.
- 435 25. De Blasiis, M.R., Di Benedetto, A., Fiani, M., Mobile Laser Scanning Data for the Evaluation of Pavement  
436 Surface Distress, **2020**, *Remote Sensing*, 12, 942.
- 437 26. Barbarella, M., D'Amico, F., De Blasiis, M.R., Di Benedetto, A., Fiani, M., Use of Terrestrial Laser Scanner  
438 for Rigid Airport Pavement Management, **2017**, *Sensors*, 18, 44.
- 439 27. Colesanti C, Ferretti A, Prati C, Rocca, F., Monitoring landslides and tectonic motions with the Permanent  
440 Scatterers Technique, *Eng Geol*, **2003**, 68(1–2):3–14,
- 441 28. Colombo D., Farina, P., Moretti, S., Nico, G., Prati, C., Land subsidence in the Firenze-Prato-Pistoia basin  
442 measured by means of spaceborne SAR interferometry. In: IGARSS 2003. 2003 IEEE international  
443 geoscience and remote sensing symposium. Proceedings (IEEE Cat. No. 03CH37477), vol 7(C), pp 2927–  
444 2929, **2003**
- 445 29. Frattini P, Crosta GB, Allievi J., Damage to buildings in large slope rock instabilities monitored with the  
446 PSinSAR™ technique, **2013**, *Remote Sensing*, 5(10), 4753–4773.
- 447 30. Yu, B., Liu, G., Zhang, R. et al. Monitoring subsidence rates along road network by persistent scatterer SAR  
448 interferometry with high-resolution TerraSAR-X imagery. *J. Mod. Transport.*, **2013**, 21, 236–246 ().
- 449 31. Perissin D., Wang Z., & Lin H., Shanghai subway tunnels and highways monitoring through Cosmo-  
450 SkyMed Persistent Scatterers. *ISPRS Journal of Photogrammetry and Remote Sensing*, **2012**, 73, 58–67.
- 451 32. Fárová, K., Jelének, J., Kopačková-Strnadová, V., Kycl, P. Comparing DInSAR and PSI Techniques  
452 Employed to Sentinel-1 Data to Monitor Highway Stability: A Case Study of a Massive Dobkovičky  
453 Landslide, Czech Republic. *Remote Sensing*. **2019**, 11, 2670.
- 454 33. Milillo P., Giardina G., Perissin D., Milillo G., Coletta A., Terranova C. Pre-collapse space geodetic  
455 observations of critical infrastructure: the Morandi Bridge, Genoa, Italy. *Remote Sensing*, **2019**;11(12):1403.
- 456 34. D'Amico F., Gagliardi V., Bianchini Ciampoli L., Tosti F., Integration of InSAR and GPR Techniques for  
457 Monitoring Transition Areas in Railway Bridges. *NDT&E International*, **2020**, In press.
- 458 35. Alani A. M., Tosti F., Bianchini Ciampoli L., Gagliardi V., Benedetto A., Integration of GPR and InSAR  
459 methods for the health monitoring of masonry arch bridges. *NDT&E International*. **2020**, In press.
- 460 36. Jung J., Kim D-J, Palanisamy Vadivel SK, Yun S-H. Long-term deflection monitoring for bridges using X  
461 and C-band time-series SAR interferometry. *Remote Sens* **2019**;11(11), 1258. 715.
- 462 37. Bianchini Ciampoli L., Gagliardi V., Calvi A., D'Amico F., Tosti F., Automatic network-level bridge  
463 monitoring by integration of InSAR and GIS catalogues. *Proceedings of SPIE - The International Society for*  
464 *Optical Engineering*, **2019**
- 465 38. Roccheggiani, M.; Piacentini, D.; Tirincanti, E.; Perissin, D.; Menichetti, M. Detection and Monitoring of  
466 Tunneling Induced Ground Movements Using Sentinel-1 SAR Interferometry. *Remote Sens*. **2019**, 11, 639.
- 467 39. Barla G. et al., InSAR monitoring of tunnel induced ground movements. *Geomechanik und Tunnelbau*, **2016**,  
468 9(1):15–22.
- 469 40. Yang Z., Schmid F., Roberts C., Assessment of railway performance by monitoring land subsidence. In: 6th  
470 IET conference on railway condition monitoring (RCM 2014), pp 1–6., **2014**.
- 471 41. Chang L, Dollevoet RPB, Hanssen RF, Nationwide railway monitoring using satellite SAR interferometry.  
472 *IEEE Journal of Selected Topics in Applied Earth Observations and Remote Sensing*, **2017**, 10, 596–604.
- 473 42. Qin X., Liao M., Zhang L., & Yang M., Structural Health and Stability Assessment of High-Speed Railways  
474 via Thermal Dilation Mapping with Time-Series InSAR Analysis. *IEEE Journal of Selected Topics in Applied*  
475 *Earth Observations and Remote Sensing*, **2017**, 10(6), 2999–3010.
- 476 43. Tosti F., Gagliardi V., D'Amico F., Alani A.M., Transport infrastructure monitoring by data fusion of GPR  
477 and SAR imagery information. *Transp Res Proc*; **2020**, 45:771-778.
- 478 44. Jiang L., & Lin H., Integrated analysis of SAR interferometric and geological data for investigating long-  
479 term reclamation settlement of Chek Lap Kok Airport, Hong Kong. *Engineering Geology*, **2010**, 110(3-4), 77–  
480 92.
- 481 45. Gao M., Gong H., Chen B., Zhou C., Chen W., Liang Y., Shi M., Si Y. InSAR time-series investigation of  
482 long-term ground displacement at Beijing Capital International Airport, China. *Tectonophysics*, **2016**, 691,  
483 271–281.

- 484 46. Jiang, Y.; Liao, M.; Wang, H.; Zhang, L.; Balz, T. Deformation Monitoring and Analysis of the Geological  
485 Environment of Pudong International Airport with Persistent Scatterer SAR Interferometry. *Remote Sens.*  
486 **2016**, *8*, 1021.
- 487 47. Sarmap. SARscape technical description. [http://www.sarmap.ch/pdf/SAR\\_scapeTechnical.pdf/](http://www.sarmap.ch/pdf/SAR_scapeTechnical.pdf/). [Accessed  
488 22 July 2020].
- 489 48. Sarmap. SAR-guidebook. <http://www.sarmap.ch/pdf/SAR-Guidebook.pdf>. [Accessed 22 July 2020]
- 490 49. NASA. The Shuttle Radar Topography Mission (SRTM) collection user guide.  
491 [https://lpdaac.usgs.gov/documents/179/SRTM\\_User\\_Guide\\_V3.pdf](https://lpdaac.usgs.gov/documents/179/SRTM_User_Guide_V3.pdf); 2015. accessed 11 February 2020.
- 492 50. Rodriguez E, Morris CS, Belz JE, Chapin EC, Martin JM, Daffer W, Hensley S. An assessment of the SRTM  
493 topographic products. Pasadena, California: Jet Propulsion Laboratory; **2005**. p. 143. Technical Report JPL  
494 D-31639.
- 495 51. Giraldo R., Delicado P., & Mateu J., Ordinary kriging for functionvalued spatial data. *Environ Ecol Stat*,  
496 **2011**, *18*, 411–426.
- 497 52. Papritz A., Stein A. Spatial prediction by linear kriging. In: Stein A., Van der Meer F., Gorte B. (eds) Spatial  
498 Statistics for Remote Sensing. *Remote Sensing and Digital Image Processing*, **1999**, vol 1. Springer, Dordrecht.
- 499 53. Doin, M.-P., C. Lasserre, G. Peltzer, O. Cavalié, and C. Doubre, Corrections of stratified tropospheric delays  
500 in SAR interferometry: Validation with global atmospheric models, *J. Appl. Geophys.*, **2009**, *69*(1), 35– 50
- 501 54. Fattahi H. and Amelung F. InSAR bias and uncertainty due to the systematic and stochastic tropospheric  
502 delay, *JGR Solid Earth*, **2015**, *10*(12), 8758-8773.
- 503



© 2019 by the authors. Submitted for possible open access publication under the terms and conditions of the Creative Commons Attribution (CC BY) license (<http://creativecommons.org/licenses/by/4.0/>).